

# UAVD4L: A Large-Scale Dataset for UAV 6-DoF Localization

Rouwan Wu<sup>1\*</sup> Xiaoya Cheng<sup>1\*</sup> Juelin Zhu<sup>1</sup> Xuxiang Liu<sup>1</sup> Maojun Zhang<sup>1†</sup>

Shen Yan<sup>1</sup>

<sup>1</sup>National University of Defense Technology  
ChangSha, China

{wurouwan97, chengxy, zhujuelin, liuyuxiang17, mjzhang, yanshen12}@nudt.edu

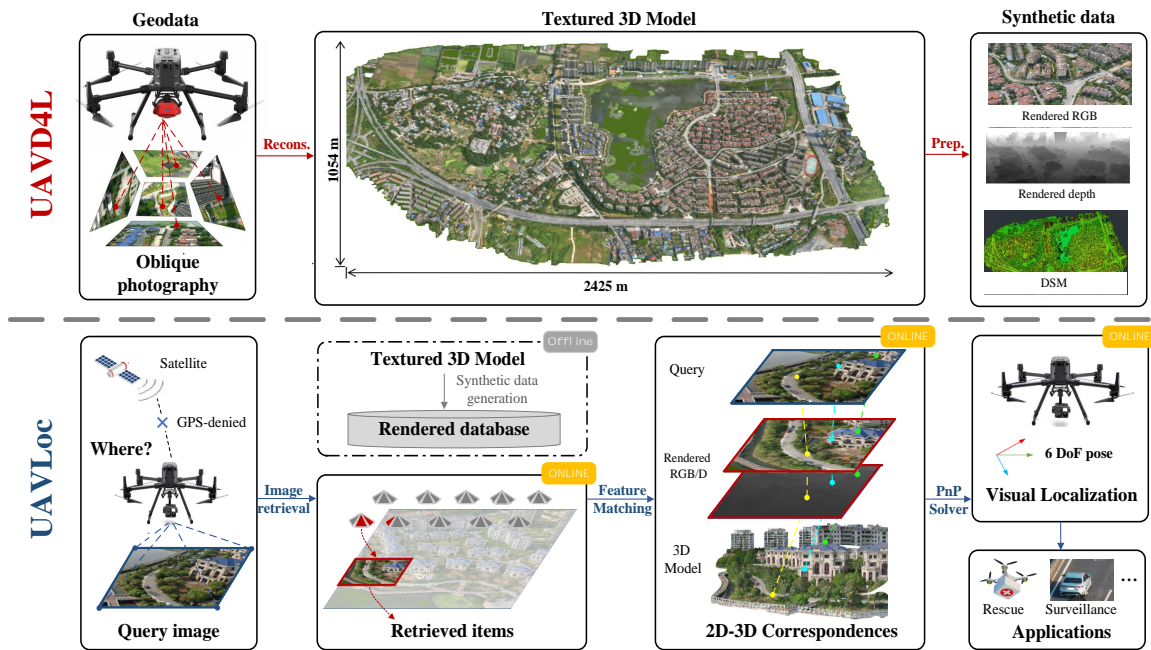


Figure 1. **Top.** We introduce a large-scale dataset for the 6-DoF localization of UAVs. The dataset includes a 3D reference textured model, which enables the generation of synthetic data such as rendered RGB and depth images, as well as a Digital Surface Model (DSM). **Bottom.** We also develop an offline-and-online pipeline for performing 6-DoF localization of UAVs in GPS-denied environments.

## Abstract

Despite significant progress in global localization of Unmanned Aerial Vehicles (UAVs) in GPS-denied environments, existing methods remain constrained by the availability of datasets. Current datasets often focus on small-scale scenes and lack viewpoint variability, accurate ground truth (GT) pose, and UAV build-in sensor data. To address these limitations, we introduce a large-scale 6-DoF UAV dataset for localization (UAVD4L) and develop a two-stage 6-DoF localization pipeline (UAVLoc),

which consists of offline synthetic data generation and online visual localization. Additionally, based on the 6-DoF estimator, we design a hierarchical system for tracking ground target in 3D space. Experimental results on the new dataset demonstrate the effectiveness of the proposed approach. Code and dataset are available at <https://github.com/RingoWRW/UAVD4L>.

## 1. Introduction

Global localization of Unmanned Aerial Vehicles (UAVs) plays an important role in various applications such as cargo

<sup>†</sup>Corresponding author: Maojun Zhang.

\*Equal contribution.

transport [25], surveillance [19], and search-rescue tasks [5, 41]. While most established works rely on global satellite navigation systems (GNSS) [3, 11, 28] for global position, vulnerabilities in GNSS signal reception [1, 22, 45] have led to the development of visual solutions [32] for GPS-denied environments.

However, compared with ground-level localization of cellphones or VR devices [34, 36, 38], the development of visual localization of UAVs lags behind. We believe this is partly due to the scarcity of open-source datasets for localizing airborne platforms in the academic community. Among the most evaluated open-source datasets, limitations include restricted to small scenes [10], evaluation of only 3-DoF positions [53], limited viewpoint variability [17], lack of accurate ground truth (GT) [20], concentration on learning-based regression methods [47], and disregard for additional inertial sensors [29].

To facilitate research in this area, our first contribution is to introduce a **novel large-scale dataset for 6-DoF UAV localization**, as shown in the top part of Figure 1. The dataset comprises a textured 3D reference model reconstructed from aerial oblique photography, covering approximately 2.5 million square meters. It enables the generation of various synthetic data, including rendered RGB and depth images, and a Digital Surface Map (DSM). Query images are captured and sampled from five distinct flight trajectories, with varying heights (50-200 meters), viewpoints (pitch angles of 15-70 degrees), and acquisition positions. Rather than relying on built-in sensor information from the UAV, such as Global Positioning System (GPS) or Real-time kinematic (RTK), to provide 3-DoF ground truth positions, we use manual tie points to register query sequences to the reference map for more accurate 6-DoF ground truth poses. In addition, sensor data (i.e., the rotation priors from the Inertial Measurement Unit (IMU)) is recorded to assist further localization algorithms.

Second, we develop a new **two-stages 6-DoF UAV localization pipeline for GPS-denied environments**, which consists of offline synthetic data generation and online visual localization, as illustrated in the bottom portion of Figure 1. In the offline stage, our approach employs rendering techniques to obtain synthetic views and depth maps at different virtual viewpoints (with varying heights and directions) to fully represent the dense 3D model of the scene. In the online stage, inspired by the recent ground-level visual localization method, SensLoc [48], we combine camera information with prior data from UAV equipment. Specifically, we first use rotation information from the built-in IMU to constrain search space for identifying relevant reference views of the query image. Then, feature matches between the query image and the top- $k$  retrieved database images are established and lifted to 2D-3D correspondences with the help of depthmaps. Finally, a gravity-guided PnP

RANSAC [7, 21] is employed to estimate the camera pose.

Finally, based on the 6-DoF localization results of UAVs, we design a **hierarchical system to track designated objects located on the ground**, such as pedestrians or vehicles. This system employs a wide-angle lens (offering a larger field of view) to determine the 6-DoF pose of the UAV, and a zoom lens to identify targets, facilitating more accurate target extraction on the 2D image. A ray-tracing technique [21] is utilized to project 2D targets on image plane onto their absolute positions in the 3D map.

## 2. Related Work

### 2.1. Ground-level Visual Localization

Conventionally, most established methods [34, 36, 37, 48] perform ground-level visual localization by establishing 2D-3D correspondences between the query image and the reconstructed sparse point clouds. The camera pose is then recovered using a PnP solver [14, 26] with RANSAC [15]. To scale to large scenes, an image retrieval phase [2, 16, 18] is often used to identify a small set of potentially relevant database images. Recently, HLoc [36, 37] has provided a comprehensive toolbox that integrates existing methods and achieves a promising result. To address the robustness, efficiency, and flexibility issues of HLoc, subsequent research includes replacing the sparse point clouds with dense model [34], and introducing sensor prior information [39, 48].

Inspired by these works, we propose a two-stage pipeline that effectively explores synthetic view representation of the dense model and successfully combines sensor prior with visual signal for localizing the 6-DoF pose of UAVs.

### 2.2. GPS-denied UAV Localization

Compared with ground-level visual localization, pose estimation of UAVs in GPS-denied environments has received less attention. Some previous works [44, 46, 49, 50] treat UAV localization as a scene recognition task, where the goal is to identify the most similar images to a query image within a geo-tagged database. The performance of this approach is influenced by the density and distribution of images within the database and can result in significant errors. Other works [6, 9, 27, 33, 47] aim to calculate the 6-DoF camera pose and can be broadly classified into two categories. The first category [40, 47] involves using neural networks to implicitly encode the scene and regress an absolute pose for an input image. These methods have the advantage of occupying small memory and having fast inference time, but their localization accuracy is limited. The second category [8] follows HLoc [36, 37] to explicitly use the map to render synthetic views upon Google Earth and recovers 6-DoF pose via image retrieval, feature matching and PnP RANSAC. Our work is similar to the second one, but we

Name	Reference source	UAV viewpoint	Map size	Estimated pose DoF	Ground truth	Open source
Chen et al. [8]	Google Earth	arbitrary	$400 \times 400m^2$	6-DoF	GPS and IMU	no
Goforth et al. [17]	United States Earth	top view	$0.85km$	6-DoF	RTK-GPS and IMU	yes
Kinnari et al. [23]	georeferenced orthophotos	arbitrary	$200 \times 200m^2$	6-DoF	RTK-GPS and IMU	yes
Kinnari et al. [24]	Google Earth	arbitrary	-	3-DoF (x,y,heading)	RTK-GPS and IMU	no
Patel et al. [35]	Google Earth	top view	$300 \times 350m^2$	4-DoF (x,y,z,heading)	RTK-GPS and IMU	no
Gurgu et al. [20]	Google Earth	top view	-	2-DoF (x,y)	RTK-GPS	yes
Zheng et al. [53]	Google Earth and Google Map	arbitrary	-	2-DoF (x,y)	sim from Google Earth	yes
Yan et al. [47]	render and real geographic image	arbitrary	2.7 million $m^2$	6-DoF	RTK-GPS and ground control point	yes
Cisneros et al. [10]	LiDAR, real image	arbitrary	$50 \times 50m^2$	6-DoF	RTK-GPS and ground control point	yes
Ours	3D model, geographic image, DSM	arbitrary	2.5 million $m^2$	6-DoF	RTK-GPS and ground control point	yes

Table 1. **Overview of the existing UAV localization datasets.** Several key attributes are taken into account: the source of reference data, the viewpoint, degrees of freedom used to measure the estimated pose, how to acquire ground truth data, and whether or not the dataset is open source.

explore richer rendering viewpoints to represent the scene, and make full use of sensor priors to achieve more accurate 6-DoF localization of UAVs.

### 2.3. UAV Localization Datasets

The development of UAV localization research is largely driven by the availability of datasets, as summarized in Table 1. However, existing UAV datasets face several challenges that limit their effectiveness in advancing the field. These challenges include: 1) **Limited Degrees of Freedom.** Many datasets, such as University-1652 [53] and ALTO [10], provide only 3 degrees of freedom (DoF) for localization, which may not be sufficient for certain applications. 2) **Top-View Bias.** Some datasets, such as those presented in [17] and [20], focus exclusively on top-view images generated from Google Earth or real drones. However, these datasets do not represent the diverse scenarios of real-world UAV usage. 3) **Regression-Based Approaches.** Datasets such as CrossLoc [47] provide rich data sources including real images, synthetic images, and semantic information for regression-based localization approaches. However, these approaches may not be suitable for structure-based localization algorithms.

These challenges highlight the need for more comprehensive and diverse datasets to advance the field of UAV localization.

## 3. Dataset

We present a large-scale dataset, UAVD4L, that covers an area of approximately 2.5 million square meters and includes a diverse range of urban and rural scenes, including buildings, streets, vegetation, and a lake. A visualization of the dataset is provided in Figure 2.

### 3.1. Reference Map Collection

To create the reference map, we captured high-resolution aerial images  $\{I_o\}$  using a DJI M300 RTK drone equipped



Figure 2. **Distribution of query images.** The query sequence consists of five trajectories, with the first four covering urban areas characterized by a high density of buildings, while the fifth trajectory covers a rural area with predominantly vegetation. The red locators, numbered from 1 to 5, represent the shooting positions.

with a five-eye oblique SHARE PSDK 102s camera. To ensure sufficient and uniform coverage of the area, we pre-planned a grid fashion flight path, which was automatically executed by the drone’s flight control system. We then applied modern 3D reconstruction techniques to produce textured mesh models and align them with the real geographic coordinate system using built-in RTK measurements and ground control points. More details about reference map collection is provided in the supplementary materials.

### 3.2. Query Image Collection

We collect all query images  $\{I_q\}$  using a DJI M300 RTK mounted with a DJI H20T camera. To enhance the diversity of query images, we manually captured images cross different regions, flight altitudes and a diverse range of capturing angles. In addition, to simulate the different shooting habits of drone pilots, we captured query images using two modes: continuous shooting at 2-second intervals and random manual shooting. The supplementary material provides statistics on the number of query images for each trajectory.

<https://enterprise.dji.com/cn/matrice-300>

<https://shareuav.cn/V3S>

<https://enterprise.dji.com/cn/zenmuse-h20-series>

### 3.3. Query GT Generation

In this work, we adopt a scalable semi-automatic annotation method to generate pseudo GT poses for query images. Our method is capable of producing pose annotations for hundreds of query images with minimal human intervention. The main steps of the method are as follows: First, we use the Structure-from-Motion (SfM) method to separately reconstruct sparse point clouds from the oblique photographic image  $\{I_o\}$  and multiple query sequences  $\{I_q\}$ . Next, we manually select some tie-points between query sequence and the oblique photographic images and perform registration based on these tie-points. Finally, we refine SfM block using bundle adjustment to achieve a whole 3D model with oblique photographic and query images.



Figure 3. **GT poses quality on UAVD4L.** Pixel-aligned renderings of the estimated camera pose confirm that the poses are sufficiently accurate for evaluation.

To evaluate the accuracy of the reference 3D model  $\mathcal{M}$ , we report the median reprojection error and the median reprojection error per tie-point, which are 0.82 pixels and 0.62 pixels, respectively. Besides, to ensure the accuracy of the pseudo GT pose, we conduct a visual inspection, and select the images whose pseudo GT pose rendered image is aligned with the original query image. Figure 3 illuminates an example where the pixel-alignment between rendered and original query image indicates that the GT poses are accurate.

## 4. Method

Given a textured reference 3D model  $\mathcal{M}$  with real-world geographical coordinates and the sensor information  $S_q$  of query image  $I_q$ , our goal is to estimate the 6-DoF pose  $\zeta_q$  of the query image  $I_q$ . To achieve this, we propose a two-stage localization pipeline. In the first stage, the database images are rendered offline according to carefully selected virtual viewpoints (Section 4.1). In the second stage, we conduct

a 6-DoF localization pipeline online (Section 4.2). Figure 4 provides an overview of the proposed method. Furthermore, based on the results of UAV 6-DoF localization, we design a hierarchical system capable of tracking ground targets in 3D space (Section 4.3).

### 4.1. Synthetic Data Generation.

Unlike ground-level localization situations, query image  $I_q$  and oblique images  $\{I_o\}$  are often captured at drastically varying positions and directions, posing a significant challenge for image retrieval [2, 16, 18] and feature matching algorithms [4, 31, 42]. To address this challenge, inspired by view synthesis work [30, 43, 47, 51, 52], we generate comprehensive synthetic reference data, including RGB images  $\{I_r\}$  and depth maps  $\{D_r\}$ , to represent the dense map of the scene.

Specifically, we first leverage the geographical boundary of 3D map  $\mathcal{M}$  to identify the area where view synthesis is required. Then the synthetic data generation can be divided into two parts: 1) For translation, we arrange the virtual viewpoints  $\zeta$  above the 3D map and establish two hyperparameters for horizontal interval distance of  $\alpha_t$  and vertical height of  $H$ , which are dynamically adjusted to ensure a uniform coverage of the entire geographic region. 2) For rotation, we set multiple  $\theta_{pitch}$  and an appropriate interval  $\alpha_{theta}$  of yaw to cover  $360^\circ$  at the same position. Based multi view and multi height render method, it can enhance adaptation to the scale invariance and rotational invariance of query images.

### 4.2. Visual Localization

**Rotation-guided image retrieval.** Given a query image  $I_q$ , we aim to identify a set of commonly visible images  $^s\mathcal{I} = \{I_{r1}, I_{r2}, \dots, I_{rk}\}$  within the reference images  $\{I_r\}$ , where  $k$  represents the number of retrieved items. A general solution involves mapping the images  $I_q, \{I_r\}$  into a compact feature space using an embedding function  $f(\cdot)$ , followed by searching for the nearest neighbors of  $I_q$  using the distance metric  $d(f(I_q), f(I_r))$ . However, simply using a global feature to find retrieved items may lead to some mistakes, as different UAV images share significant viewpoint and scale changes.

To improve the retrieval accuracy, inspired by SensLoc [48], we use the metadata from UAV sensors  $S$ , especially the rotation information, as a prior to pre-filter incorrect reference candidates. Considering a richer variety of viewpoints in drones, we impose constraints on each degree of rotation angle, consisting of  $\theta_{roll}$ ,  $\theta_{yaw}$ ,  $\theta_{pitch}$ , as shown in Equation 1.

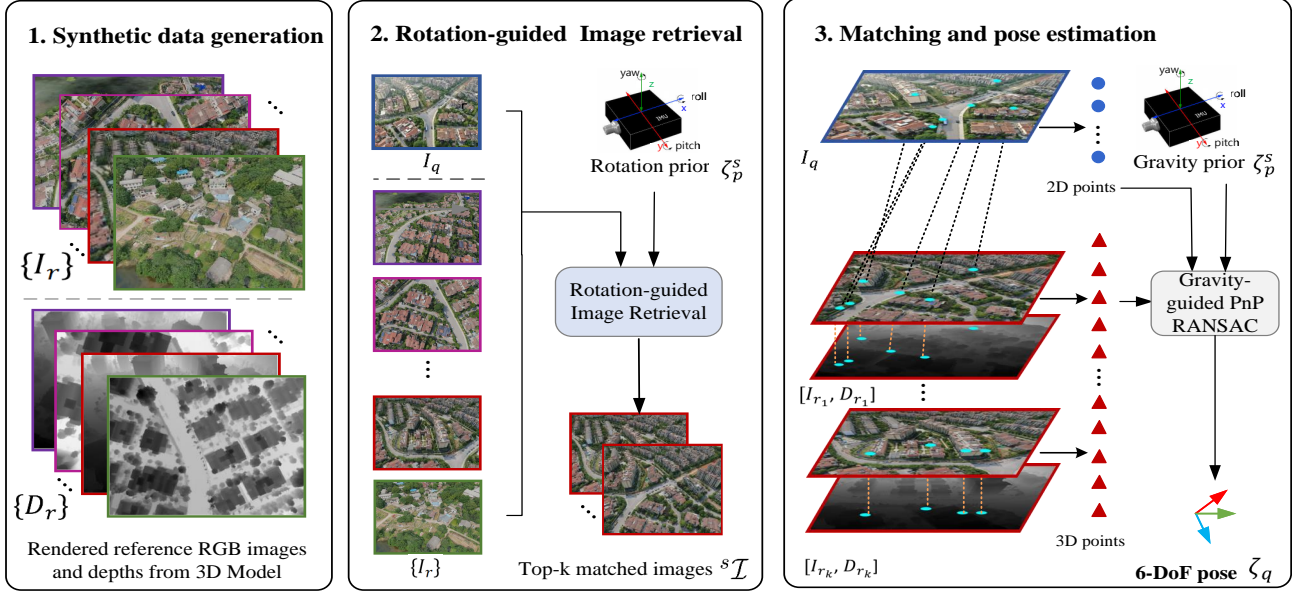


Figure 4. **Overview of the proposed method.** 1. We generate comprehensive synthetic data from textured 3D model, including RGB images  $I_r$  and depthmaps  $D_r$  (Section 4.1). 2. For each query image  $I_q$ , we use an image retrieval algorithm combined with rotation sensor prior  $S$  to find the top- $k$  relevant images. 3. Then, we apply feature detection and matching algorithm to establish the 2D-3D correspondence between the query image  $I_q$  and the relevant images  $I_r$ . A gravity-guided PnP RANSAC is used to obtain the pose  $\zeta_q$  of the UAV (Section 4.2).

$$\begin{aligned}
 & \left\| -\arcsin(R_{31}^S) - \theta_{roll}^r \right\| \leq \gamma_o, \\
 & \left\| \arctan\left(\frac{R_{21}^S}{R_{11}^S}\right) - \theta_{yaw}^r \right\| \leq \gamma_o, \\
 & \left\| \arctan\left(\frac{R_{32}^S}{R_{33}^S}\right) - \theta_{pitch}^r \right\| \leq \gamma_o, \\
 & R_{31}^S \neq \pm 1,
 \end{aligned} \tag{1}$$

where  $\gamma_o$  is a orientation threshold and  $R^S$  represents the rotation matrix from the sensor prior  $S$ .  $\theta^r$  represents the rotation angle of the reference image. After pre-filtering incorrect candidate data using rotation information as a prior, we are able to efficiently and accurately determine  $k$  nearest neighbor  ${}^s\mathcal{I}$  according to  $d(f(I_q), f({}^p\mathcal{I}))$ .

**Matching and pose estimation.** We adopt learnable feature matching techniques to establish 2D-2D correspondences between the query image  $I_q$  and the retrieved synthetic images  ${}^s\mathcal{I}$ . Since depthmaps  ${}^s\mathcal{D}$  are also rendered during the offline stage of synthetic data generation, these 2D-2D correspondences can be lifted to 2D-3D correspondences via back-projection.

For pose estimation, we follow SensLoc [48] and incorporate a gravity verification module into the PnP RANSAC process. During each RANSAC iteration, we compute the deviation  $d_\epsilon$  between the gravity direction of the sensor pose

$\zeta_s^g$  and the hypothetical pose  $\zeta_{hyp}^g$ , as shown in Equation 2. If this deviation  $d_\epsilon$  is less than a predefined stopping threshold  $\gamma_\epsilon$ , we halt the RANSAC iterations prematurely.

$$d_\epsilon = \arccos(\zeta_s^g \cdot \zeta_{hyp}^g) \tag{2}$$

### 4.3. Hierarchical Target Tracking

Based on the proposed 6-DoF UAV pose estimation approach mentioned above, we design a hierarchical system for target tracking on the ground, as illustrated in Figure 5.

The system comprises two cameras: a fixed wide-angle lens camera and a zoom lens camera, which are carefully calibrated. The wide-angle lens, with a broader vision for global and local feature extraction, captures images for on-line 6-DoF localization. The zoom lens captures images for specific target detection, where the target occupies a sufficient area. Afterwards, the 3D position of the target is estimated using ray-tracing [7, 21] based on a digital elevation model (DEM), as detailed in the supplementary material.

### 4.4. Implementation Details

In the offline synthetic reference data generation process, we generate virtual viewpoints with absolute altitude  $H = 100m$  and  $150m$ , the horizontal interval  $\alpha_t = 50m$  and  $\alpha_t = 75m$ , respectively, and generate 16 images with different angles ( $\theta_{pitch}^r = 0^\circ$  or  $45^\circ$ ,  $\alpha_{theta} = 45^\circ$ ) for each

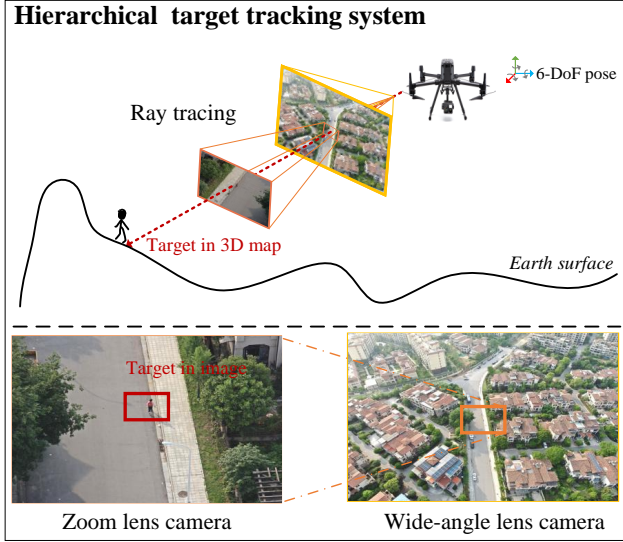


Figure 5. **The hierarchical target tracking system** consists of two lens: a wide-angle lens camera and a zoom lens camera. The wide-angle lens camera is used to recover the 6-DoF pose of the UAV, while the zoom lens camera is used to accurately detect the target. A ray-tracking technique is employed to track designated targets in 3D space.

same position. In the image retrieval step, the angle threshold  $\gamma_o$  is set to  $30^\circ$ . In the gravity-guided PnP solver step, we set the gravity angle threshold  $\gamma_\epsilon = 2^\circ$ . We perform all experiments on a PC equipped with Intel Core i9-11900K processor, GTX 3090 graphics card (24 GB RAM) and Ubuntu 18.04 operating system. We implement the proposed pipeline in Python alone with Pytorch.

## 5. Experiment

### 5.1. Image Retrieval

**Baselines.** In this study, we evaluate the performance of several global descriptors at image retrieval stage, including NetVLAD [2], AP-GeM [18], and OpenIBL [16]. Additionally, we conduct controlled experiments to verify the effectiveness of using a rotation sensor prior.

**Evaluation protocol.** Retrieval results are considered correct if they share a sufficient overlapping area with the query image, where the overlap percentage  $P_{overlap}$  is greater than 50%. The overlap area between two images is calculated by transforming pixels from one image to the other based on their depth maps. Please refer to the supplementary materials for more details.

**Results.** The retrieval results are shown in Table 2. We maintain a rank list of size  $k$  for each query and report re-

call and precision metrics. The experimental results show that all three representative retrieval methods are capable of finding correct retrieved items, even when the rotation sensor is not adapted. This can be attributed to the generation of comprehensive virtual views across the scene, which contributes to the availability of more visual similar images. Among all options, OpenIBL [16] with rank list  $k = 3$  and employing sensor priors leads the benchmark, and is chosen to find a visible reference set in the localization pipeline.

Global feature	Prior	R@1	R@3	P@3
NetVLAD [2]	-	73.6	98.08	74.42
	Rot	<b>79.9</b>	98.08	<b>77.8</b>
AP-GeM [18]	-	84.62	96.5	72.55
	Rot	<b>85.31</b>	<b>97.55</b>	<b>73.14</b>
OpenIBL [16]	-	83.74	98.43	76.69
	Rot	<b>84.44</b>	<b>98.78</b>	<b>79.08</b>

Table 2. **Image retrieval results.** We report the top- $k$  recall and precision for  $k = 1, 3$ , using global image features and considering the use of rotation priors.

### 5.2. Visual Localization

**Baselines.** We evaluate the performance of various keypoint descriptors, including SIFT [12] and Superpoint [13], as well as matchers such as Nearest Neighbor and the learnable SuperGlue [37]. We also compare the results with those obtained using the detector-free matcher LoFTR [42]. For pose estimation, we employ the PnP RANSAC solver, with and without gravity information.

**Evaluation protocol.** Our evaluation follows the standard localization benchmark protocol [38, 47], reporting results under the thresholds of  $(1m, 1^\circ)$ ,  $(3m, 3^\circ)$  and  $(5m, 5^\circ)$ .

**Results.** The quantitative results are presented in Table 3. The Superpoint+Superglue outperforms other counterparts in all metric except  $(1m, 1^\circ)$ . This may be attributed to the fact that query images of UAVD4L were taken under favorable lighting conditions and feature rich textures that facilitate keypoint detection by SuperPoint. Additionally, we found that the gravity-guided PnP RANSAC method [48] enhances localization accuracy regardless of the matching algorithm used. Qualitative results can be found in Figure 6 and Figure 7. Figure 6 provide the feature matching results, while Figure 7 provides a comparison between rendered estimated pose images and their corresponding original images, further demonstrating the precision of our results.

### 5.3. Target Tracking

To evaluate the target tracking performance of the proposed method, we capture people and car from two trajectories, and using the data recorded by RTK as their GT position.

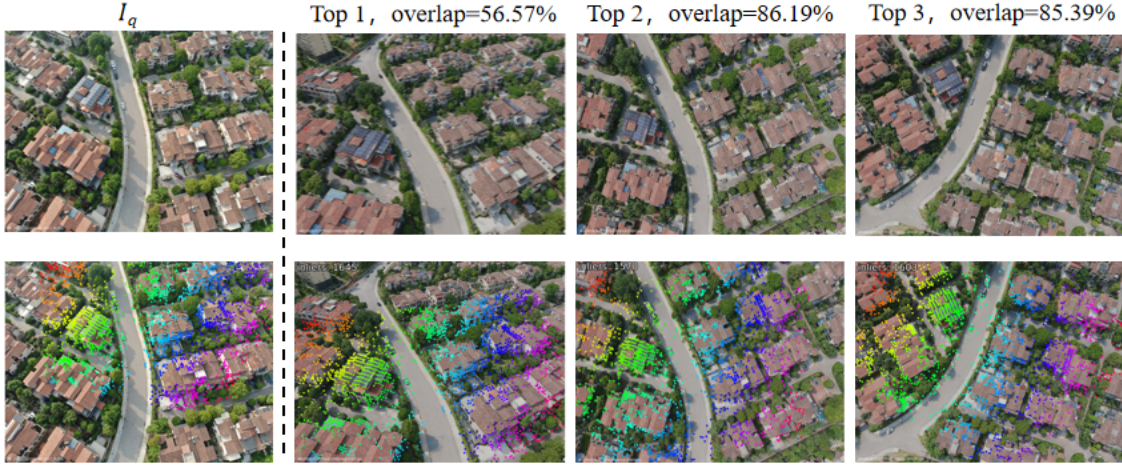


Figure 6. **Qualitative results.** The top part of the figure illustrates an example retrieval result using OpenIBL. The bottom part displays the local feature matching results by employing SuperPoint and SuperGlue. The matched correspondences are visualized using the same color scheme.

Method	-			Gravity-guided		
	$(1m, 1^\circ)$	$(3m, 3^\circ)$	$(5m, 5^\circ)$	$(1m, 1^\circ)$	$(3m, 3^\circ)$	$(5m, 5^\circ)$
LoFTR(Top @1)	39.34	89.34	89.86	43.18	91.78	93.01
LoFTR(Top @3)	41.26	93.53	93.88	43.18	93.88	94.58
SIFT + NN(Top @3)	34.79	91.26	93.01	34.09	90.73	91.78
SPP + NN(Top @3)	<b>41.96</b>	93.71	94.06	43.71	94.93	95.45
SPP + SPG(Top @3)	40.73	<b>94.76</b>	<b>94.76</b>	<b>44.58</b>	<b>96.15</b>	<b>96.68</b>

Table 3. **Visual localization results on UAVD4L.** We evaluate the localization performance of different feature detectors and descriptors using the two-stages UAV localization pipeline with /without sensor priors. Note that all methods use OpenIBL for image retrieval.

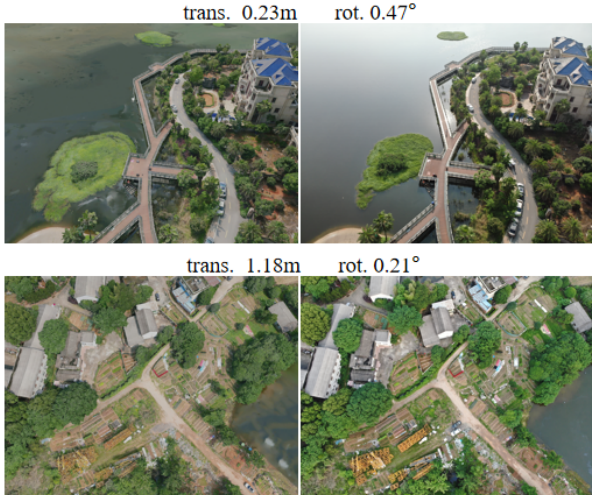


Figure 7. **Visual results of images rendered from the estimated poses.** The localization error for each pose is shown at the top of the image.

**Evaluation protocol.** We adopt the translation difference between the ground truth 3D coordinates and the computed

3D coordinates to represent the target tracking estimation error.

**Results.** Figure 8 shows two sequential UAV localization and target tracking results, with and without the use of sensor information for localization.

Due to the accurate UAV localization, the target position achieves meter-level accuracy. Figure 9 visualizes the difference between the estimated target trajectory and the true trajectory under different UAV localization results. It can be seen that target estimation using sensor-guided localization results in a smaller position error.

Hierarchical render ( $m, \circ$ )	$(1m, 1^\circ)$ / $(3m, 3^\circ)$ / $(5m, 5^\circ)$
$H = 150, \theta_{pitch}^r = 45$	32.69 / 79.2 / 79.37
$H = 150 \& 100, \theta_{pitch}^r = 45$	42.63 / 89.86 / 90.03
$H = 150 \& 100, \theta_{pitch}^r = 45 \& 0$	<b>44.58 / 96.15 / 96.68</b>

Table 4. **Ablation study.** The visual localization results of different hierarchical render setting are reported on the UAVD4L.

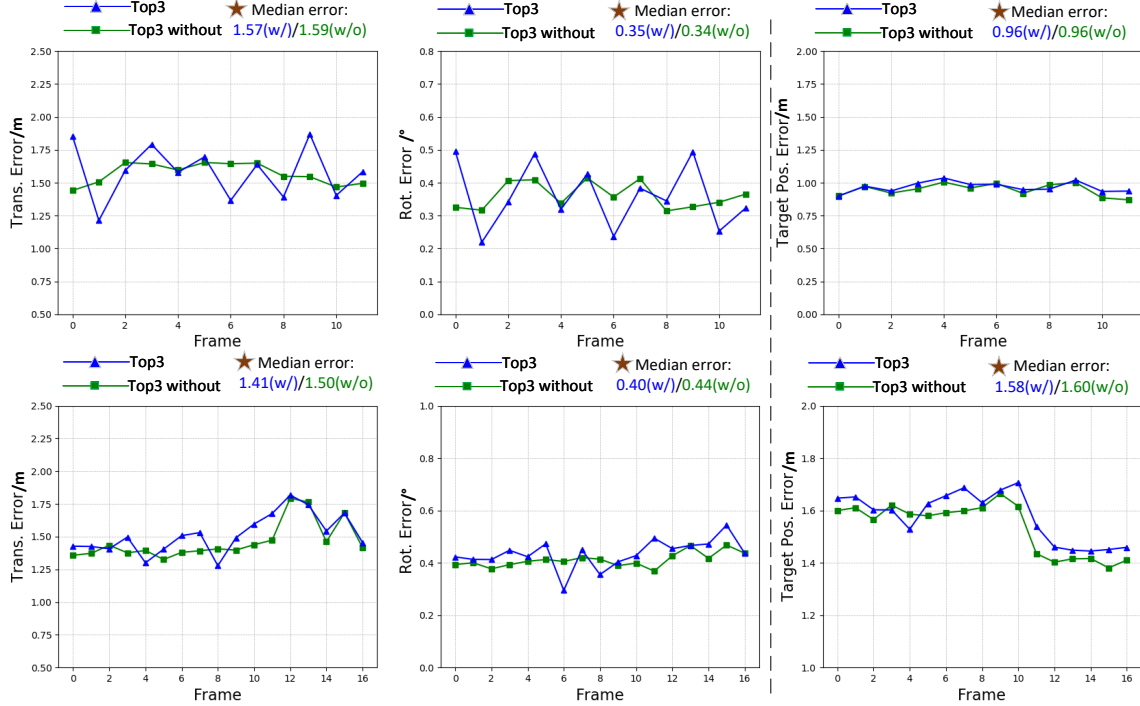


Figure 8. **Localization error results for different trajectory.** For two target tracking trajectories, we report the UAV localization and target tracking error with or without sensor prior.

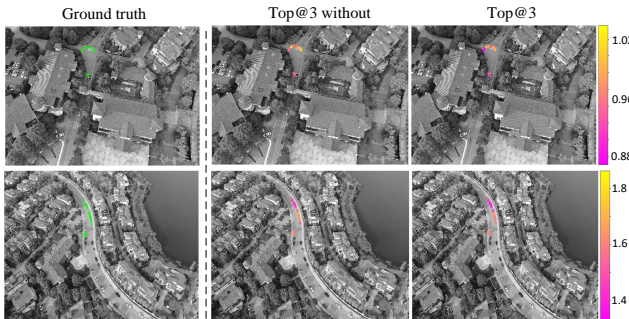


Figure 9. **Qualitative results of target tracking.** The left side of the figure displays the ground truth positions of the tracking target, represented by green points. The right side of the figure shows the estimated target position error, measured in meters as a translation error.

#### 5.4. Ablation Studies

To fully understand the impact of different hierarchical render settings on visual localization, we evaluate three render setting with results show in Table 4. Only render single level of attitude and angle obtains the lowest accuracy, while render multiple levels of attitude and angle attains the favorable accuracy. This indicates increasing render layer by attitude and angle improves the results. We conduct these ex-

periment using the same image retrieval (OpenIBL), feature point detection and matching (SPP+SPG), and the gravity-guided PnP RANSAC on UAVD4L.

## 6. Conclusion

We introduce a large-scale dataset, UAVD4L, for UAV 6-DoF localization in GPS-denied environments. The dataset contains a world-aligned textured 3D reference model and query images with accurate GT poses. However, generating an accurate GT poses of low illumination images is difficult, so in the future we will apply advanced techniques to expand our dataset. Additionally, we implement a novel two-stage 6-DoF localization pipeline that fully utilizes comprehensive data rendering and rotation sensor information. Furthermore, based on the 6-DoF pose estimator, we design a hierarchical system to track designated objects on the ground and output their 3D positions. We anticipate that the UAVD4L dataset will serve as a valuable resource and benchmark for future research in this field.

**Acknowledgements.** The authors would like to acknowledge the support from the Natural Science Foundation of Hunan Province of China (2020JJ5671).

## References

- [1] Abdulla Al-Kaff, David Martin, Fernando Garcia, Arturo de la Escalera, and José María Armingol. Survey of computer vision algorithms and applications for unmanned aerial vehicles. *Expert Sys. Appl.*, 2018. [2](#)
- [2] Relja Arandjelovic, Petr Gronat, Akihiko Torii, Tomas Pajdla, and Josef Sivic. Netvlad: Cnn architecture for weakly supervised place recognition. In *CVPR*, 2016. [2](#), [4](#), [6](#)
- [3] Ganesan Balamurugan, J Valarmathi, and VPS Naidu. Survey on uav navigation in gps denied environments. In *SCOPES*, 2016. [2](#)
- [4] Giovanni Barbarani, Mohamad Mostafa, Hajali Bayramov, Gabriele Trivigno, Gabriele Berton, Carlo Masone, and Barbara Caputo. Are local features all you need for cross-domain visual place recognition? In *CVPR*, 2023. [4](#)
- [5] Mesay Belete Bejiga, Abdallah Zeggada, Abdelhamid Noufidj, and Farid Melgani. A convolutional neural network approach for assisting avalanche search and rescue operations with uav imagery. *Remote Sens.*, 2017. [2](#)
- [6] Mollie Bianchi and Timothy D Barfoot. Uav localization using autoencoded satellite images. *IEEE Robot. Autom.*, 2021. [2](#)
- [7] Yiming Cai, Yao Zhou, Hongwen Zhang, Yuli Xia, Peng Qiao, and Junsuo Zhao. Review of target geo-location algorithms for aerial remote sensing cameras without control points. *Appl. Sci.*, 2022. [2](#), [5](#)
- [8] Shuxiao Chen, Xiangyu Wu, Mark W Mueller, and Koushil Sreenath. Real-time geo-localization using satellite imagery and topography for unmanned aerial vehicles. In *IROS*, 2021. [2](#), [3](#)
- [9] Junho Choi and Hyun Myung. Brm localization: Uav localization in gnss-denied environments based on matching of numerical map and uav images. In *IROS*, 2020. [2](#)
- [10] Ivan Cisneros, Peng Yin, Ji Zhang, Howie Choset, and Sebastian Scherer. Alto: A large-scale dataset for uav visual place recognition and localization. *arXiv preprint*, 2022. [2](#), [3](#)
- [11] Andy Couturier and Moulay A Akhloufi. A review on absolute visual localization for uav. *Rob. Autom. Syst.*, 2021. [2](#)
- [12] Lowe David. Distinctive image features from scale-invariant keypoints. *IJCV*, 2004. [6](#)
- [13] Daniel DeTone, Tomasz Malisiewicz, and Andrew Rabinovich. Superpoint: Self-supervised interest point detection and description. In *CVPR*, 2018. [6](#)
- [14] Yaqing Ding, Jian Yang, Viktor Larsson, Carl Olsson, and Kalle Åström. Revisiting the p3p problem. 2023. [2](#)
- [15] Martin A Fischler and Robert C Bolles. Random sample consensus: a paradigm for model fitting with applications to image analysis and automated cartography. *Commun. ACM*, 1981. [2](#)
- [16] Yixiao Ge, Haibo Wang, Feng Zhu, Rui Zhao, and Hongsheng Li. Self-supervising fine-grained region similarities for large-scale image localization. In *ECCV*, 2020. [2](#), [4](#), [6](#)
- [17] Hunter Goforth and Simon Lucey. Gps-denied uav localization using pre-existing satellite imagery. In *ICRA*, 2019. [2](#), [3](#)
- [18] Albert Gordo, Jon Almazan, Jerome Revaud, and Diane Larlus. End-to-end learning of deep visual representations for image retrieval. *IJCV*, 2017. [2](#), [4](#), [6](#)
- [19] Emilia Guisado-Pintado, Derek WT Jackson, and David Rogers. 3d mapping efficacy of a drone and terrestrial laser scanner over a temperate beach-dune zone. *Geomorphology*, 2019. [2](#)
- [20] Marius-Mihail Gurgu, Jorge Peña Queralta, and Tomi West-erlund. Vision-based gnss-free localization for uavs in the wild. In *ICMERR*, 2022. [2](#), [3](#)
- [21] Chao Huang, Hongmei Zhang, and Jianhu Zhao. High-efficiency determination of coastline by combination of tidal level and coastal zone dem from uav tilt photogrammetry. *Remote Sens.*, 2020. [2](#), [5](#)
- [22] Christoforos Kanellakis and George Nikolakopoulos. Survey on computer vision for uavs: Current developments and trends. *J. Intell. Rob. Syst. Theor. Appl.*, 2017. [2](#)
- [23] Jouko Kinnari, Francesco Verdoja, and Ville Kyrki. Gnss-denied geolocalization of uavs by visual matching of on-board camera images with orthophotos. In *ICRA*, 2021. [3](#)
- [24] Jouko Kinnari, Riccardo Renzulli, Francesco Verdoja, and Ville Kyrki. Lsvl: Large-scale season-invariant visual localization for uavs. *arXiv preprint*, 2022. [3](#)
- [25] Edward Larson, Arthur Ianuzzi, Renier Oliva, Dennis Lorence, Graham Sheffer, et al. Autonomous underwater survey apparatus and system, 2021. US Patent 11,072,405. [2](#)
- [26] Vincent Lepetit, Francesc Moreno-Noguer, and Pascal Fua. Eppn: An accurate o(n) solution to the pnp problem. *IJCV*, 2009. [2](#)
- [27] Yu Liu, Jing Bai, Gang Wang, Xiaobo Wu, Fangde Sun, Zhengqiang Guo, and Hujun Geng. Uav localization in low-altitude gnss-denied environments based on poi and store signage text matching in uav images. *Drones*, 2023. [2](#)
- [28] Yuncheng Lu, Zhucun Xue, Gui-Song Xia, and Liangpei Zhang. A survey on vision-based uav navigation. *Geo-Spatial Inf. Sci.*, 2018. [2](#)
- [29] Alina Marcu, Dragos Costea, Emil Slusanschi, and Marius Leordeanu. A multi-stage multi-task neural network for aerial scene interpretation and geolocalization. *arXiv preprint*, 2018. [2](#)
- [30] Arthur Moreau, Nathan Piasco, Dzmitry Tsishkou, Bogdan Stanculescu, and Arnaud de La Fortelle. Lens: Localization enhanced by nerf synthesis. In *Proc. Mach. Learn. Res.*, 2022. [4](#)
- [31] Muhammad Hamza Mughal, Muhammad Jawad Khokhar, and Muhammad Shahzad. Assisting uav localization via deep contextual image matching. *IEEE J. Sel. Top. Appl. Earth Obs. Remote Sens.*, 2021. [4](#)
- [32] Ahmed Nassar and Mohamed ElHelw. Aerial imagery registration using deep learning for uav geolocalization. In *CVPRW*, 2018. [2](#)
- [33] Nipun D Nath, Chih-Shen Cheng, and Amir H Behzadan. Drone mapping of damage information in gps-denied disaster sites. *Adv. Eng. Inf.*, 2022. [2](#)
- [34] Vojtech Panek, Zuzana Kukelova, and Torsten Sattler. Meshloc: Mesh-based visual localization. In *ECCV*, 2022. [2](#)

- [35] Bhavit Patel, Timothy D Barfoot, and Angela P Schoellig. Visual localization with google earth images for robust global pose estimation of uavs. In *ICRA*, 2020. 3
- [36] Paul-Edouard Sarlin, Cesar Cadena, Roland Siegwart, and Marcin Dymczyk. From coarse to fine: Robust hierarchical localization at large scale. In *CVPR*, 2019. 2
- [37] Paul-Edouard Sarlin, Daniel DeTone, Tomasz Malisiewicz, and Andrew Rabinovich. Superglue: Learning feature matching with graph neural networks. In *CVPR*, 2020. 2, 6
- [38] Paul-Edouard Sarlin, Ajaykumar Unagar, Mans Larsson, Hugo Germain, Carl Toft, Viktor Larsson, Marc Pollefeys, Vincent Lepetit, Lars Hammarstrand, Fredrik Kahl, et al. Back to the feature: Learning robust camera localization from pixels to pose. In *CVPR*, 2021. 2, 6
- [39] Paul-Edouard Sarlin, Mihai Dusmanu, Johannes L Schönberger, Pablo Speciale, Lukas Gruber, Viktor Larsson, Ondrej Miksik, and Marc Pollefeys. Lamar: Benchmarking localization and mapping for augmented reality. In *ECCV*, 2022. 2
- [40] Akshay Shetty and Grace Xingxin Gao. Uav pose estimation using cross-view geolocalization with satellite imagery. In *ICRA*, 2019. 2
- [41] Mario Silvagni, Andrea Tonoli, Enrico Zenerino, and Marcello Chiaberge. Multipurpose uav for search and rescue operations in mountain avalanche events. *Geomatics Nat. Hazards Risk*, 2017. 2
- [42] Jiaming Sun, Zehong Shen, Yuang Wang, Hujun Bao, and Xiaowei Zhou. Loftr: Detector-free local feature matching with transformers. In *CVPR*, 2021. 4, 6
- [43] Hajime Taira, Masatoshi Okutomi, Torsten Sattler, Mircea Cimpoi, Marc Pollefeys, Josef Sivic, Tomas Pajdla, and Akihiko Torii. Inloc: Indoor visual localization with dense matching and view synthesis. In *CVPR*, 2018. 4
- [44] Songbing Wu, Chun Du, Hao Chen, and Ning Jing. Coarse-to-fine uav image geo-localization using multi-stage lucaskanade networks. In *ICTC*, 2021. 2
- [45] Yingxiao Xu, Long Pan, Chun Du, Jun Li, Ning Jing, and Jiangjiang Wu. Vision-based uavs aerial image localization: A survey. In *SIGSPATIAL*, 2018. 2
- [46] Yingxiao Xu, Songbing Wu, Chun Du, Jun Li, and Ning Jing. Uav image geo-localization by point-line-patch feature matching and iclk optimization. In *Int. Conf. Geoinformatics*, 2022. 2
- [47] Qi Yan, Jianhao Zheng, Simon Reding, Shanci Li, and Jordan Doytchinov. Crossloc: Scalable aerial localization assisted by multimodal synthetic data. In *CVPR*, 2022. 2, 3, 4, 6
- [48] Shen Yan, Yu Liu, Long Wang, Zehong Shen, Zhen Peng, Haomin Liu, Maojun Zhang, Guofeng Zhang, and Xiaowei Zhou. Long-term visual localization with mobile sensors. In *CVPR*, 2023. 2, 4, 5, 6
- [49] Peng Yin, Lingyun Xu, Ji Zhang, Howie Choset, and Sebastian Scherer. i3dloc: Image-to-range cross-domain localization robust to inconsistent environmental conditions. *arXiv preprint*, 2021. 2
- [50] Peng Yin, Ivan Cisneros, Shiqi Zhao, Ji Zhang, Howie Choset, and Sebastian Scherer. isimloc: Visual global localization for previously unseen environments with simulated images. *IEEE Trans. Rob.*, 2023. 2
- [51] Jiahui Zhang, Shitao Tang, Kejie Qiu, Rui Huang, Chuan Fang, Le Cui, Zilong Dong, Siyu Zhu, and Ping Tan. Rendernet: Visual relocalization using virtual viewpoints in large-scale indoor environments. *arXiv preprint*, 2022. 4
- [52] Zichao Zhang, Torsten Sattler, and Davide Scaramuzza. Reference pose generation for long-term visual localization via learned features and view synthesis. *IJCV*, 2021. 4
- [53] Zhedong Zheng, Yunchao Wei, and Yi Yang. University-1652: A multi-view multi-source benchmark for drone-based geo-localization. In *MM*, 2020. 2, 3